aerospace

MDPI

Article

Microvibration Suppression for the Survey Camera of CSST

Renkui Jiang [1], Wei Liang [1], Libin Wang [1], Enhai Liu [1], Xuerui Liu [2], Yongchao Zhang [1], Sixian Le [1], Zhaoyang Li [1], Hongyu Wang [3], Tonglei Jiang [4], Changqing Lin [1], Shaohua Guan [1], Weiqi Xu [1], Haibing Su [1], Yanqing Zhang [1], Junfeng Du [1] and Ang Zhang [1,*]

[1] Institute of Optics and Electronics, Chinese Academy of Sciences, Chengdu 610209, China; jiangrenkui@ioe.ac.cn (R.J.); liangwei@ioe.ac.cn (W.L.); lb_wang0811@163.com (L.W.); liuenhai@ioe.ac.cn (E.L.); zhangyongchao@ioe.ac.cn (Y.Z.); lesixian@ioe.ac.cn (S.L.); lizhaoyang@ioe.ac.cn (Z.L.); linchangqing@ioe.ac.cn (C.L.); guanshaohua@ioe.ac.cn (S.G.); xuweiqi@ioe.ac.cn (W.X.); shb@ioe.ac.cn (H.S.); adazhang1201@163.com (Y.Z.); junfeng_du2012@163.com (J.D.)

[2] Shanghai Institute of Technical Physics of the Chinese Academy of Sciences, Shanghai 200003, China; liuxuerui@ioe.ac.cn

[3] Changchun Aerospace Composite Materials Co., Ltd., Changchun 130102, China; wanghy_2026@163.com

[4] National Time Service Center, Chinese Academy of Sciences, Xi'an 710600, China; tonglei87@mail.nwpu.edu.cn

* Correspondence: zhangang@ioe.ac.cn

Abstract

The Survey Camera (SC) is the key instrument of the China Space Station Telescope (CSST), with its imaging performance significantly constrained by microvibrations from internal sources such as the shutter and cryocoolers. This paper proposes a systematic microvibration suppression scheme integrating disturbance source control, payload isolation, and transfer path optimization to meet the stringent requirements. The Cryocooler Assembly (CCA) compressor adopts a symmetric piston layout and a real-time vibration cancellation algorithm to reduce the vibration. Coupled with a vibration isolator designed by combining hydraulic damping and a flexible structure, it achieves a vibration isolation efficiency of 95%. The shutter adopts dual-blade symmetric design with sinusoidal angular acceleration control, ensuring its vibrations fall within the compensable range of the Fast Steering Mirror (FSM). And the finite element optimization method is used to optimize the dynamic characteristics of the Support Structure (SST) made of M55J carbon fiber composite material, to avoid resonance in the critical frequency bands. System-level tests on the integrated SC show that the RMS values of vibration force and torque within 8–300 Hz are 0.25 N and 0.08 N·m, respectively, meeting design specifications. This scheme validates effective microvibration control, guaranteeing the SC's high-resolution imaging capability for the CSST mission.

Keywords: microvibration suppression; vibration isolation; cryocooler; shutter; China Space Station Telescope

Check for updates

Academic Editor: Hyun-Ung Oh

Received: 8 December 2025
Revised: 5 January 2026
Accepted: 7 January 2026
Published: 8 January 2026

Copyright: © 2026 by the authors. Licensee MDPI, Basel, Switzerland. This article is an open access article distributed under the terms and conditions of the Creative Commons Attribution (CC BY) license.

1. Introduction

As the core payload of the CSST (as illustrated in Figure 1), the SC undertakes 70% of the telescope's observational tasks, with its observational wavelength coverage spanning 255–1000 nm. The total pixel count for both its scientific observation and guide star wavefront sensing reaches 3.3 billion—surpassing that of the GAIA telescope, making it the highest-pixel space astronomical camera to date [1]. To fulfill the CSST's high-precision

observation mission, the radius encircling 80% energy of the point spread function (PSF) within the central 1.1 square degrees of the field of view is required to be no more than 0.15″ (at λ = 632.8 nm) [2]. This stringent index encompasses all optical wavefront errors and dynamic disturbances, among which microvibrations induced by the SC's internal components (shutter and CCA) have emerged as a critical limiting factor for imaging performance. During the exposure process, microvibrations from these internal sources are transmitted to the CSST platform, causing jitter of the telescope's optical axis and relative displacement between the observed target and the detector, which ultimately degrades the spatial resolution of the acquired images.

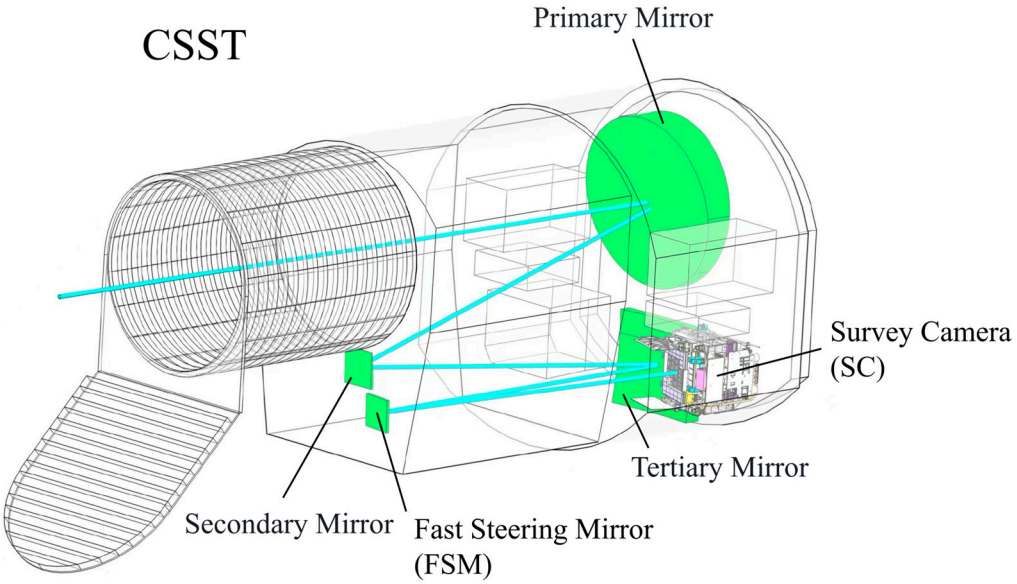


Figure 1. The CSST and Survey Camera.

Unlike space telescopes such as JWST [3], GAIA [4], Kepler [5], and HST [6], the SC integrates a large-area focal plane array while accommodating two dominant internal vibration sources with distinct characteristics, leading to multiple challenges for microvibration control: the vibration sources are diverse, the transmission paths of vibrations through the support structure are complex, the overall system exhibits strong dynamic coupling effects, and the vibration frequency band (8–300 Hz) exceeds the compensation range of the FSM configured in the CSST optical system. For such a high-precision and complex opto-mechanical system, relying on a single microvibration suppression method is insufficient to meet the stringent requirements of the CSST mission.

Microvibration suppression for spacecraft payloads typically involves three technical routes—disturbance source suppression, payload isolation, and transmission path optimization [7]—each targeting different links in the vibration transmission chain. Disturbance source suppression focuses on reducing vibration excitation at the source by optimizing the structural design and operational parameters of internal components [8,9]; for instance, the Euclid telescope's shutter adopts a dynamically balanced blade design to minimize operational microvibrations [10,11]. Payload isolation establishes a flexible connection between the sensitive payload and the platform by introducing damping elements or active control mechanisms, thereby blocking vibration transmission [12–14]; a representative case is the XRISM spacecraft, which employs three sets of isolator struts to isolate vibrations from its refrigeration compressors [15]. Transmission path optimization weakens vibration propagation by improving the structural dynamic characteristics of connecting components such as frames and pipelines [16]; for example, Tacsat-2 utilizes improved D-struts to optimize the vibration transmission path between its optical payload and service module [17].

While these methods have achieved successful applications in different space missions, their separate implementation fails to address the multi-source, wide-frequency-band microvibration challenges faced by the SC.

To address this critical issue, this paper proposes a systematic microvibration suppression scheme that integrates disturbance source control, payload isolation, and transmission path optimization, tailored specifically to the SC's structural features and vibration characteristics. For the CCA—the primary vibration source—we adopt a combination of symmetric piston layout, real-time vibration cancellation algorithm, and a custom-designed vibration isolator based on hydraulic damping and flexible structure, achieving a vibration isolation efficiency of 95%. For the shutter, a dual-blade symmetric design with sinusoidal angular acceleration control is implemented, ensuring that its operational vibrations fall within the FSM's compensable range. Additionally, finite element optimization is applied to the M55J carbon fiber composite support structure (SST) to adjust its dynamic characteristics, avoiding resonance amplification in critical frequency bands. System-level tests validate that the proposed scheme effectively controls the RMS values of vibration force and torque transmitted to the CSST within the 8–300 Hz band to 0.25 N and 0.08 N·m, respectively, meeting the design specifications and guaranteeing the SC's high-resolution imaging capability.

It should be noted that the CSST involves multiple on-orbit microvibration disturbance sources besides the SC, such as reaction wheels and mechanical gyroscopes, which are also potential factors inducing the vibration of telescope mirrors. The suppression of disturbances from these sources is designated as parallel research tasks by the CSST project team, with independent technical routes and implementation schemes. The present study focuses solely on the microvibration generated by the SC's internal components, and the proposed suppression scheme will synergize with the control strategies for other disturbance sources to collectively meet the stringent image stability requirements of the CSST mission.

The remainder of this paper is organized as follows: Section 2 presents the SC's mechanical architecture and the technical requirements for microvibration suppression; Section 3 elaborates on the multi-dimensional microvibration suppression and isolation scheme, including CCA vibration control, shutter low-vibration design, and SST dynamic characteristic optimization; Section 4 describes the system-level microvibration testing and verification results of the integrated SC; finally, Section 5 summarizes the key findings and conclusions of this study.

2. Materials and Methods

The SC (composed of 28 components) is integrally mounted on the Support Structure (SST)—the core load-bearing component made of M55J carbon fiber composite material, as shown in Figure 2. The Focal Plane Array (FPA) is located in the $1.1^\circ \times 1.0^\circ$ main imaging area of the survey field of view, equipped with 31 CCDs and measuring 500×600 mm in size. The Shutter (at the frontmost end) controls the camera's exposure. The Cryocooler Assembly (CCA) is installed on the camera's side, with its core function of cooling the FPA to below 185K. In the shutter-closed state, the SC has dimensions of 895 mm $\times$ 1047 mm $\times$ 1047 mm and a launch mass of 450kg [18].

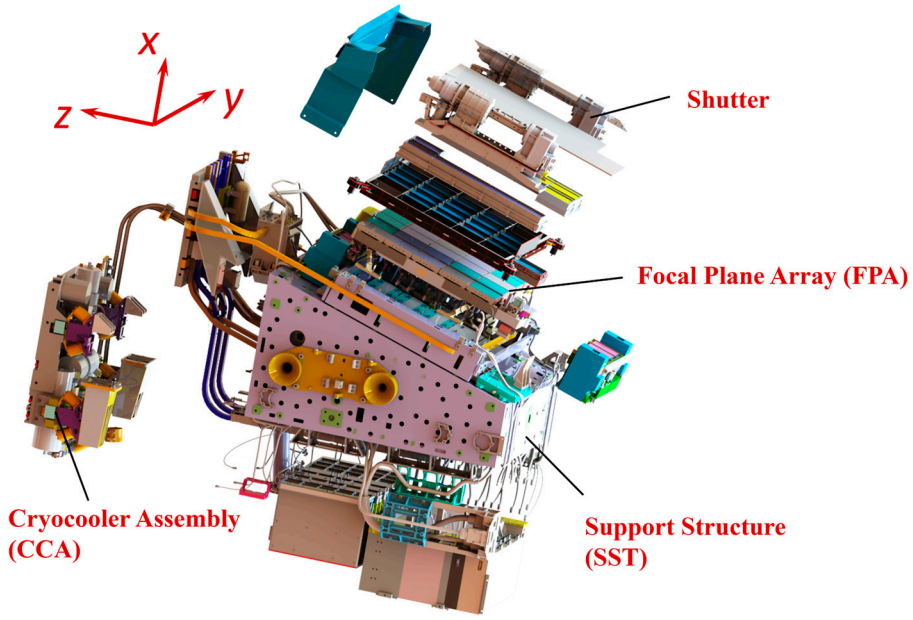


Figure 2. The SC mechanical architecture.

The four mounting interfaces (A, B, C, and D mounting interfaces, as shown in Figure 3) on the SST realize the mechanical connection between the SC and the CSST, and also serve as vibration transmission path [18].

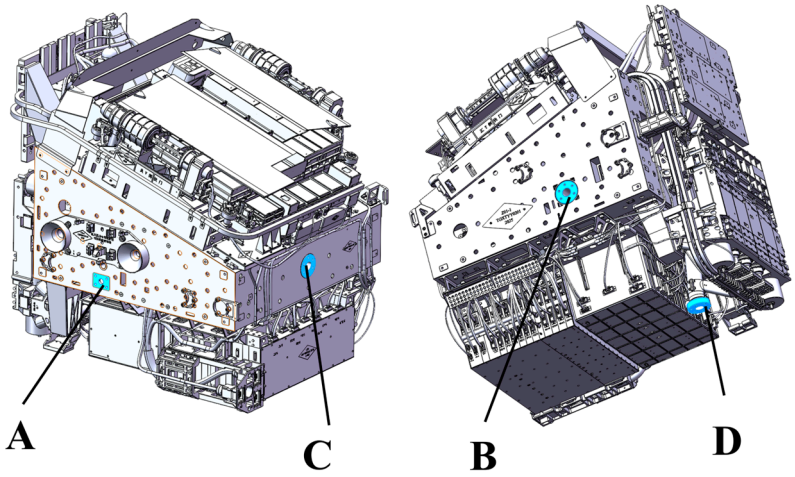


Figure 3. The mounting interface between the SC and CSST.

The FSM of the CSST configured in the optical system has precise image stabilization capability, which can effectively compensate for the impact of low-frequency vibrations below 8 Hz on imaging. However, for vibrations above 8 Hz, the dynamic response capability of the FSM is limited, making complete suppression difficult. The residual optical axis jitter after compensation by the FSM will cause displacement of the observed target relative to the detector during exposure, thereby significantly reducing the spatial resolution of the image. To ensure imaging quality, the root mean square (RMS) values of the vibration force and torque transmitted from the SC to the CSST within the 8–300 Hz frequency range must be controlled to $\leq$0.4 N and $\leq$0.1 N·m, respectively. It should be clarified that these two specifications ($\leq$0.4 N and $\leq$0.1 N·m) are not the requirements for single-direction force or torque, but refer to the resultant force and resultant torque in the three directions (x, y, z). Specifically, these mechanical requirements at the SC-CSST interface are derived from the primary opto-mechanical system: through quantitative analysis of the impact

of microvibrations on optical imaging performance, the top-level requirement for image stability is translated into the measurable force and torque constraints at the mounting interface between the SC and CSST.

3. Microvibration Suppression Scheme for the SC

3.1. Vibration Suppression and Isolation for the CCA

The CCA internally integrates four pulse tube cryocoolers (PTCs), among which three are used to cool the focal plane array to below 185 K, and one is utilized to cool the short-wave infrared detector to below 80 K. Compared with Stirling cryocooler, the PTC has no moving parts at the cold end, meaning less vibration [19], as well as advantages such as low electromagnetic interference, high reliability, and long service life [20], making them more suitable for meeting the low-vibration and 10-year service life requirements of the SC. Each PTC is equipped with a compressor featuring a symmetric piston arrangement. Through algorithm-based real-time control of piston motion, the compressor achieves active cancellation of vibration forces [21].

The vibration control principle for the compressor is depicted in Figure 4. This vibration reduction control system comprises a controller and a vibration sensor, with the controller serving as the core component that integrates external circuits and control software. The output of the controller corresponds to the driving signals for the compressor motors, while its input is the residual vibration error feedback signal (post vibration reduction)—this signal is derived from the raw vibration signal captured by the vibration sensor, following conditioning processes including amplification and filtering.

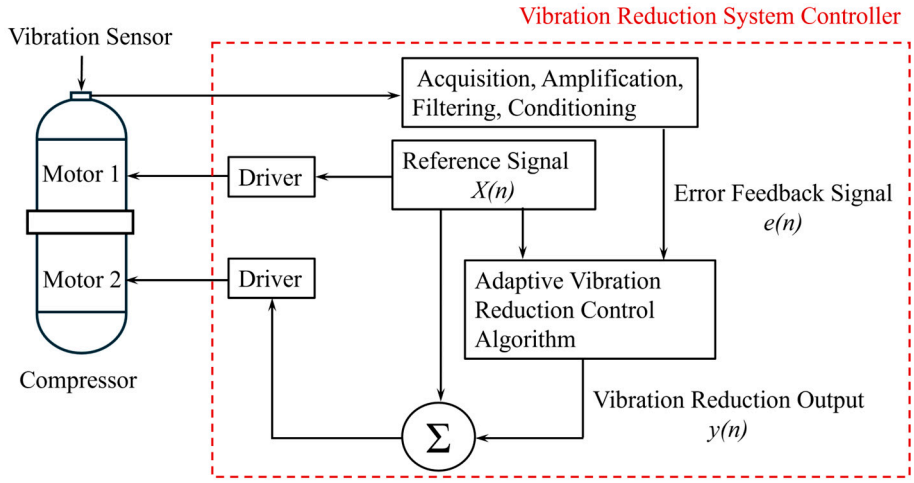


Figure 4. Control principle of adaptive vibration control for compressor.

The driving signal for the compressor is split into two branches: one branch is directly driven by the reference signal, while the other is a composite driving signal formed by superimposing the vibration reduction output signal onto the reference signal. The vibration reduction output signal generates a counter-vibration force, which neutralizes the original vibration via linear superposition with the inherent vibration force. By implementing this vibration reduction control strategy, the vibration acceleration of the compressor is reduced from 0.166 m/s^2 to 0.014 m/s^2 [21].

The operating frequency of the compressor can be adjusted within the range of 75–85 Hz, with additional vibrations occurring at its 2nd and 3rd harmonics. Although the cold head of the PTC achieves vibration-free operation, the vibration of its compressor cannot be ignored, especially when four compressors work together, resulting in significant vibration superposition. To reduce the vibration of the CCA, vibration isolators are installed between the CCA and the support structure of the SC.

The schematic diagram illustrating the working principle of the vibration isolator is presented in Figure 5. Hydraulic oil is hermetically sealed within the bellows cavity. When relative motion occurs between the excitation end and the response end, the hydraulic oil flows reciprocally through the damping orifice, generating resistance to dissipate vibration energy and thereby creating a specific damping effect. The bellows and the flexible structure at the excitation end regulate the connection stiffness of the CCA to approximately 10 Hz, enabling suppression of over 95% of the vibrations originating from the CCA [22]. Before the SC enters orbit, the vibration isolators are maintained in a locked state. This configuration ensures that the connection stiffness of the CCA meets the requirements of the severe mechanical environment during the launch phase. Once the SC has successfully entered orbit, the vibration isolators are subsequently unlocked and activate to perform their vibration isolation function.

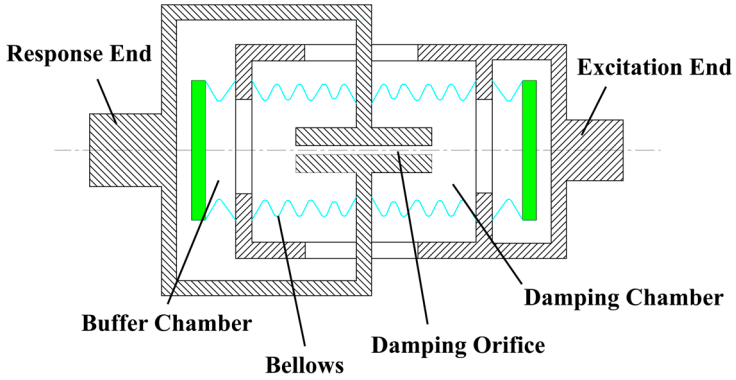


Figure 5. Schematic diagram of the Vibration Isolator.

When measuring the post-isolation vibration response of the CCA, the CCA was suspended by a spring to prevent damage to the vibration isolator and simulate a weightless environment, as shown in Figure 6.

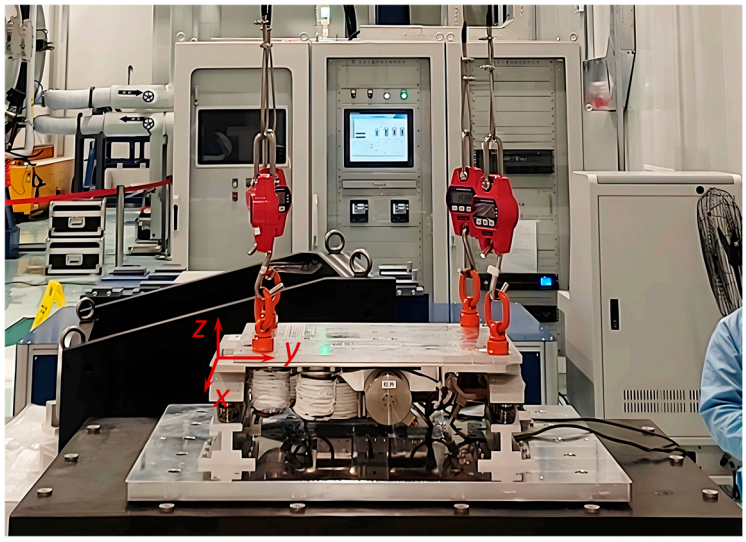


Figure 6. Testing of Cryocooler Assembly vibration force.

The vibration force spectrum curve of the CCA at a typical operating frequency of 80 Hz is presented in Figure 7, with the corresponding directions of the curves indicated in Figure 6. (It is worth noting that the directions of the coordinate systems in all figures and curves presented in this paper are consistent throughout.) It shows that the vibration force

is primarily distributed at 80Hz and its harmonics. The RMS values of the vibration force within the 8–300 Hz frequency range are only 0.20N.

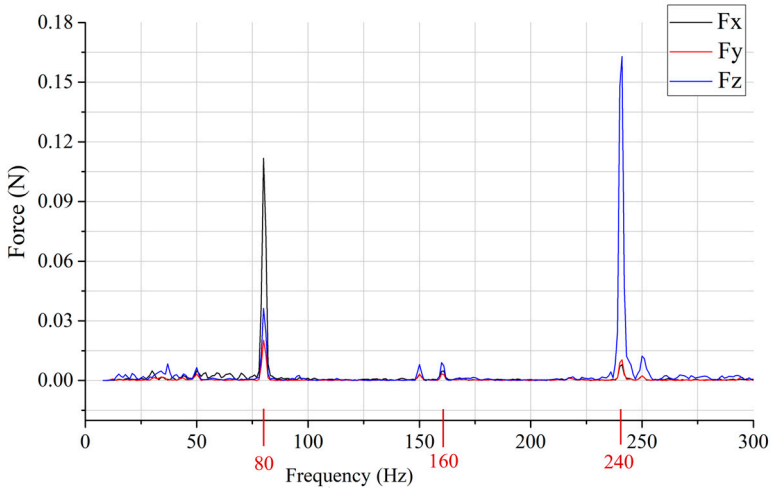


Figure 7. Measured vibration force spectrum of the Cryocooler Assembly.

3.2. Vibration Suppression for the Shutter

The shutter adopts a dual-blade rotating structure, with two carbon fiber thin plates rotating to shield the FPA, as shown in Figure 8, similar in structure to the shutter of Euclid's VIS instrument [10,11], but with more prominent technical indicators: a design life of up to ten years, an exposure area of 640 × 540mm, an opening/closing angle of 90°, and a movement cycle of only 1.5 s, featuring higher efficiency than similar products. The shutters on both sides of the SC are symmetrically arranged; each shutter mainly consists of a shaft, encoder, servo motor, blade, counterweight, locking mechanism, and on-orbit manual reset device. The encoder on the shaft can feed back the blade angle in real-time, and the coordinated control of motors on both sides realizes synchronous opening and closing of the blades; the counterweight can fine-tune the moment of inertia of the blades to ensure high consistency of the moment of inertia of the blades on both sides, thereby achieving mutual cancellation of driving torque and in-plane vibration force during operation, ensuring low-vibration operation of the shutter. The locking mechanism is used to lock the shaft, ensuring that the shutter blades maintain a preset fixed angle during transportation and launch. By setting the locking angles of the shutters on both sides, a safe distance can be formed between the two blades to avoid collision during launch.

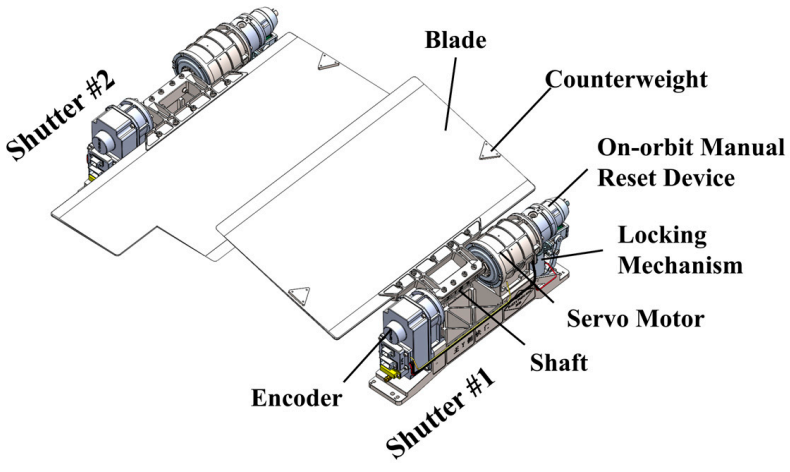


Figure 8. The shutter mechanical architecture.

The rotation of the shutter blade employs a sinusoidal angular acceleration drive control strategy, which is specifically tailored to mitigate mechanical shocks and suppress excessive vibration excitation during the transient start-up and shutdown phases of the shutter (as illustrated in Figure 9). Unlike conventional step-type control methods that tend to induce abrupt force fluctuations (a common source of microvibration in shutter systems), this strategy regulates the blade's angular acceleration to vary sinusoidally over time: as reflected in Figure 9 (covering the 0–1.5 s single operation cycle of the shutter), the sinusoidal profile of angular acceleration (black curve) drives a smooth ramp-up and ramp-down of angular velocity (blue curve), free of abrupt jumps. Correspondingly, the blade angle (red curve) exhibits a continuous, steady variation throughout the motion process. This well-regulated dynamic response not only ensures the smooth mechanical operation of the shutter during start-up and shutdown but also minimizes the vibration disturbance generated by blade motion—such low-frequency residual vibration falls within the effective compensation bandwidth of the CSST's FSM, thus eliminating adverse impacts on the camera's imaging performance.

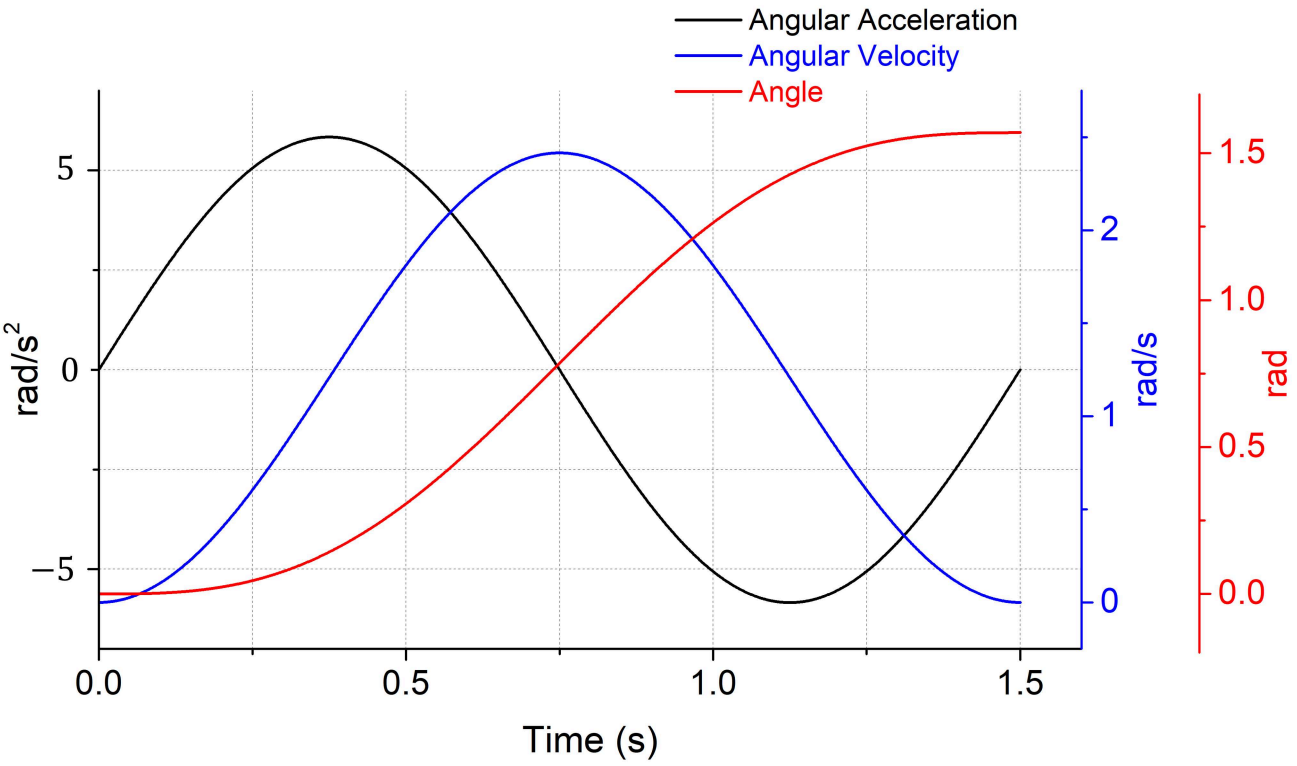


Figure 9. Drive curve of the shutter shaft.

Additionally, microvibration testing of the shutter assembly has been conducted as shown in Figure 10. Test results have indicated that its vibration attenuates rapidly after the shutter is fully opened or closed, and the 1.5-s working cycle of the shutter results in a very low vibration frequency, which is within the effective compensation bandwidth of the telescope's FSM (8 Hz). For the typical exposure time of 150 s of the SC, the vibration generated during shutter operation has no impact on camera imaging.

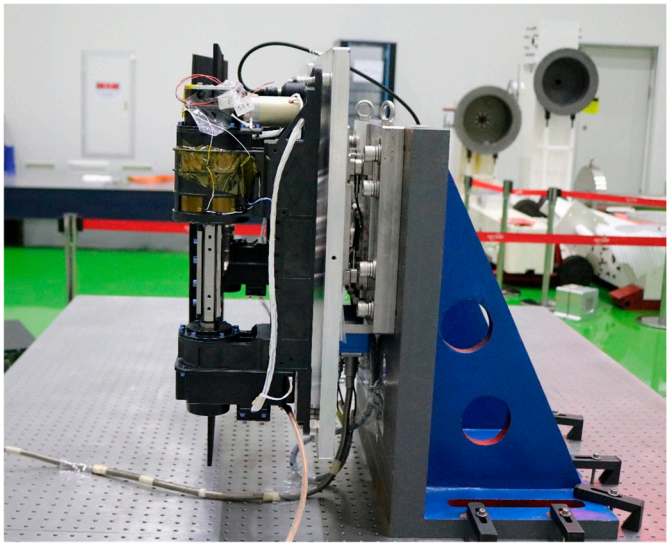


Figure 10. Testing of shutter vibration force.

3.3. Dynamic Characteristics Optimization of the SST

The SST, as the core load-bearing component of the SC, is integrally formed using M55J carbon fiber composite material [18]. Figure 11 presents a local sectional view of the SST. This material effectively ensures structural lightweighting by virtue of its high specific stiffness [23]; simultaneously, its high damping property provides an inherent advantage for microvibration suppression. To guarantee the connection reliability and strength of each interface, titanium alloy inserts are pre-embedded at all connection positions, achieving a high-strength bond between the composite material and metal parts, which significantly enhances the overall stiffness and load-bearing capacity of the structure.

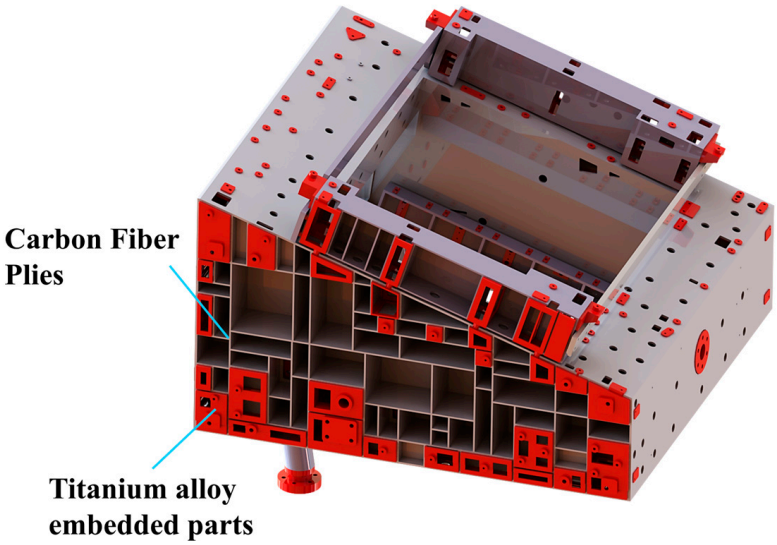


Figure 11. Local sectional view of the SST.

The SST serves as the main path for vibration transmission from the CCA to the CSST. To avoid resonance amplification effects caused by the coupling of the camera's natural frequencies with excitation, a systematic optimization of the dynamic characteristics of the SST was conducted based on finite element analysis (FEA).

The CCA operates at an adjustable frequency range of 75–85 Hz, and its vibration spectrum additionally contains prominent components at the 2nd and 3rd harmonics of this fundamental frequency band. To account for potential frequency deviations in

actual operating conditions (e.g., operational fluctuations, assembly tolerances) and ensure robust vibration suppression performance, the SST is required to maintain high dynamic stability across the extended frequency intervals of 70–90 Hz, 140–180 Hz, and 210–270 Hz (providing sufficient margin to cover the CCA's fundamental frequency and its harmonics).

To this end, a systematic optimization of the SST's dynamic characteristics was implemented: Given the SST's complex carbon fiber composite structure, the carbon fiber layup thicknesses of its internal reinforcing ribs and outer skins were selected as optimization variables (the total number of variables exceeded 150, attributed to the intricate structural details). A dual-objective optimization criterion was established: maximizing the SST's overall fundamental frequency to enhance structural stiffness, and minimizing its vibration response amplitude within the target frequency ranges to weaken vibration transmission. Furthermore, in alignment with the lightweight requirements of the CSST mission, the upper mass limit of the SST ($\leq$68 kg) was set as a key constraint. Through the solution of this multi-variable, multi-objective optimization problem, the dynamic properties of the SST were precisely regulated—this ensures that the structural stiffness meets load-bearing requirements, while also significantly suppressing the resonance peaks in the SST's vibration transmission curve within the target frequency intervals. The multi-variable optimization of the SST was implemented based on the Size Optimization Module (SOL 200) of MSC Nastran. To improve optimization efficiency, individual mass points were used to replace each component, ensuring that the inertia of the model is consistent with that of the SC, as shown in Figure 12.

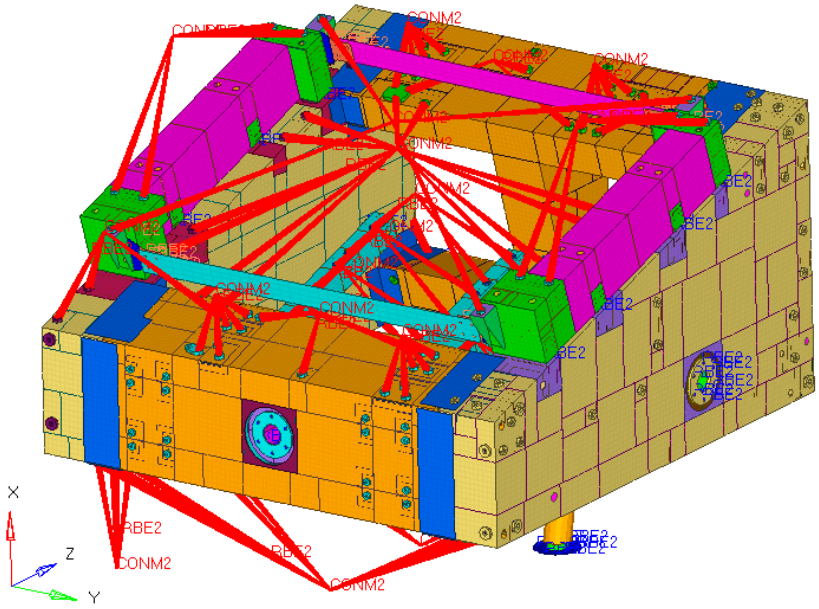


Figure 12. Finite element model of the SST.

As shown in Figure 13, after optimization, within the target frequency ranges, the resonance peaks in the vibration force transmission curve from the CCA to the CSST via the SST are effectively shifted and suppressed, enabling the SST to successfully block the amplified transmission of microvibrations.

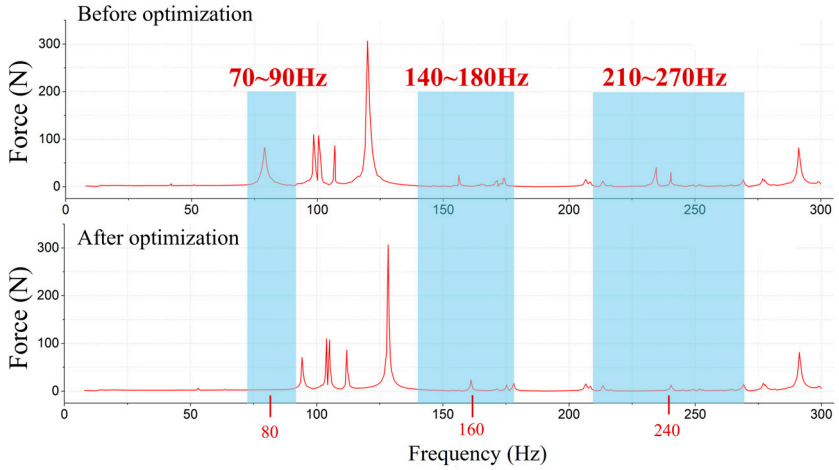


Figure 13. Vibration transmissibility curves of the SST before and after optimization.

Upon application of vibration excitation of the CCA (with a typical operating frequency of 80 Hz) to the optimized finite element model of the SST, the frequency curve of the vibration force response at the SC mounting interface was computed, as illustrated in Figure 14. Within the frequency range of 8–300 Hz, the RMS values of the vibration force and torque are 0.19 N and 0.06 N·m, respectively. Compared with the 0.20 N excitation generated by the CCA, the vibration force was not amplified during its transmission through the SST. This result validates that the optimized design of the SST's dynamic characteristics has effectively mitigated the risk of resonance amplification, ensuring the stability of vibration in the transmission path.

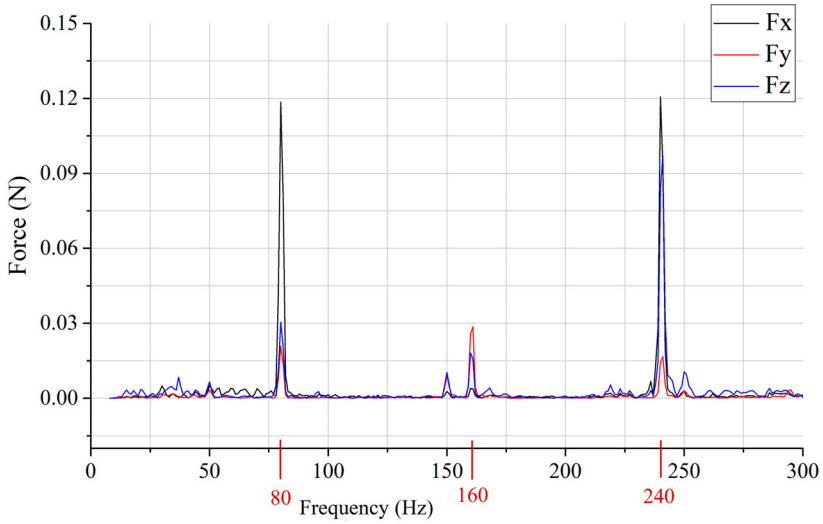


Figure 14. Vibration force response spectrum of the SC mounting interface.

Further extraction of the vibration displacement responses at the centroid of the FPA (as shown in Figure 15) indicates that the vibration amplitude is controlled below 4 nm, a value that is far smaller than 1/100 of the pixel size and thus will not affect imaging. Collectively, these analyses demonstrate that the optimization of the dynamic characteristics of the SST has effectively suppressed energy coupling in the vibration transmission path from the CCA.

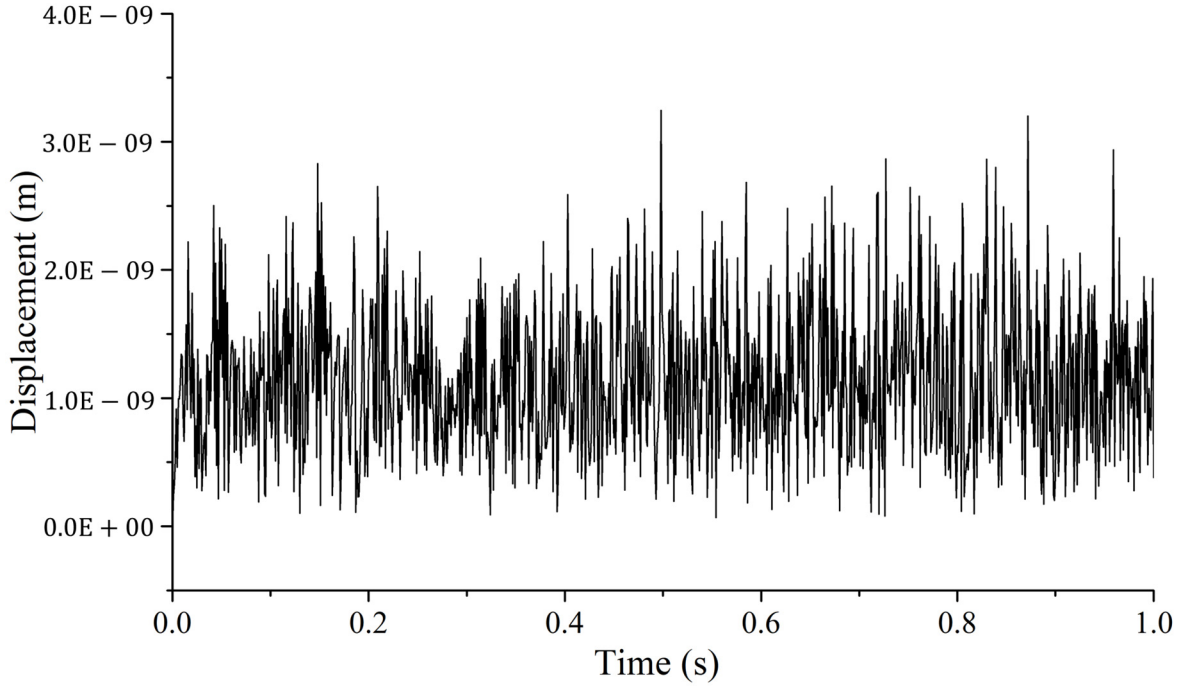


Figure 15. Vibration displacement response of the FPA center of mass point.

4. Microvibration Testing of the SC

Figure 16 shows the fully integrated camera. As the first system-level test after the camera's integration, microvibration testing is crucial for verifying its dynamic performance.

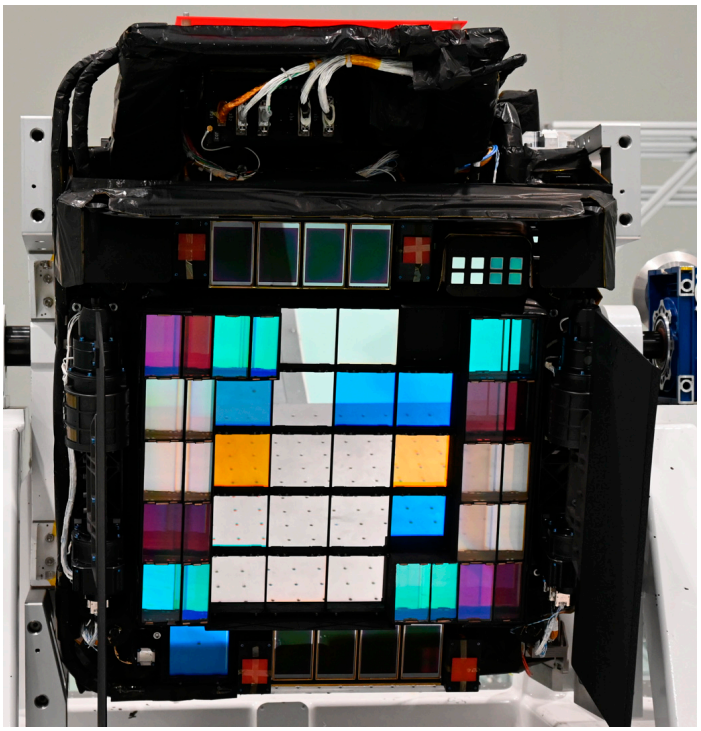


Figure 16. The fully integrated Survey Camera.

To meet the microvibration testing requirements of the SC, a dedicated Microvibration Testing System (MVTS) was developed, as shown in Figure 17. The system integrates four Kistler 9347C force sensors, which are symmetrically installed between the ground foundation and the carbon fiber mounting base plate [24]. The SC is connected to the

mounting base plate via a dedicated connecting fixture. Through multi-sensor coupled measurement technology, combined with charge amplifiers and a data acquisition system, the testing system achieves high-precision measurement capabilities of 0.005 N for force and 0.001 N·m for torque within the measurement ranges of 600 N (force) and 12 N·m (torque).

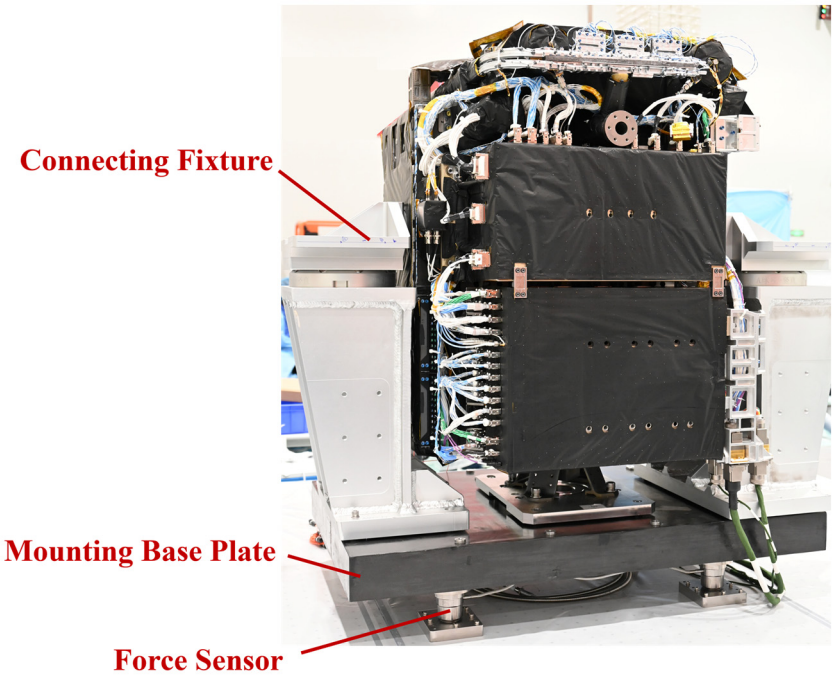


Figure 17. Microvibration Testing System.

After testing and data processing, the time-domain response curves of the vibration force and torque of the Survey Camera (SC) are shown in Figure 18. Within the 8–300 Hz frequency range, the root mean square (RMS) values of the vibration resultant force and torque were 0.25 N and 0.08 N·m, respectively, which meet the specifications of the SC (i.e., vibration force $\leq$ 0.4 N and torque $\leq$ 0.1 N·m) [24]. From the spectral characteristics (as shown in Figure 19), it is observed that the characteristic vibration excitations of the cryocooler at 80 Hz, 160 Hz, and 240 Hz did not undergo amplitude amplification after transmission through the SST—this confirms the suppression effect of the SST dynamic characteristic optimization on vibration propagation. However, a comparison between the analytical results and the measured data indicates that the measured spectrum presents an additional prominent vibration response in the 250–300 Hz frequency range. The discrepancy between these two sets of results can be attributed to the following aspects: First, during the analytical process, each functional component of the SC was replaced by equivalent mass points in the model, which led to insufficient consideration of the inherent dynamic characteristics of the individual components. Second, the actual SC incorporates a variety of auxiliary structures (e.g., heat pipes, cables, thermal blankets, etc.). When the cryocooler's vibration is transmitted to these components and auxiliary structures via the SST, it triggers resonance in some of these parts, thereby giving rise to the extra vibration response in the 250–300 Hz frequency band. Nevertheless, the overall vibration response level meets the expected requirements.

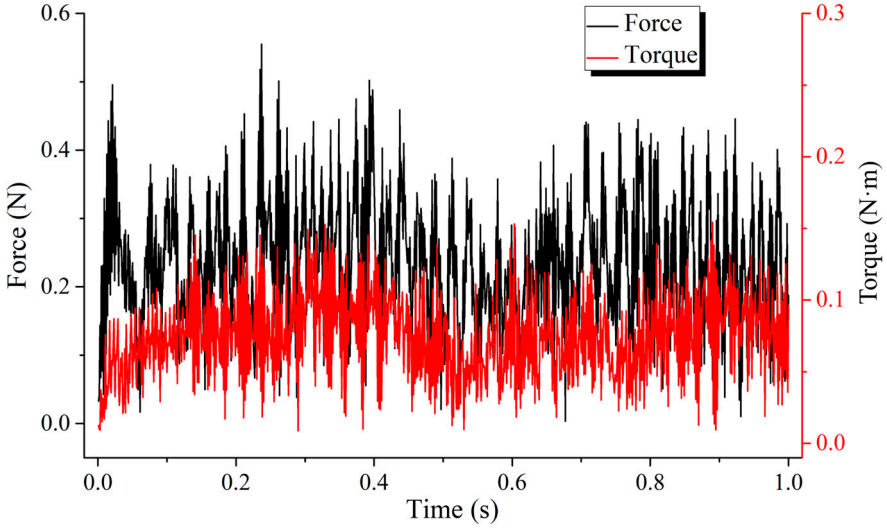


Figure 18. Measured time-domain responses of the vibration resultant force and torque of the SC.

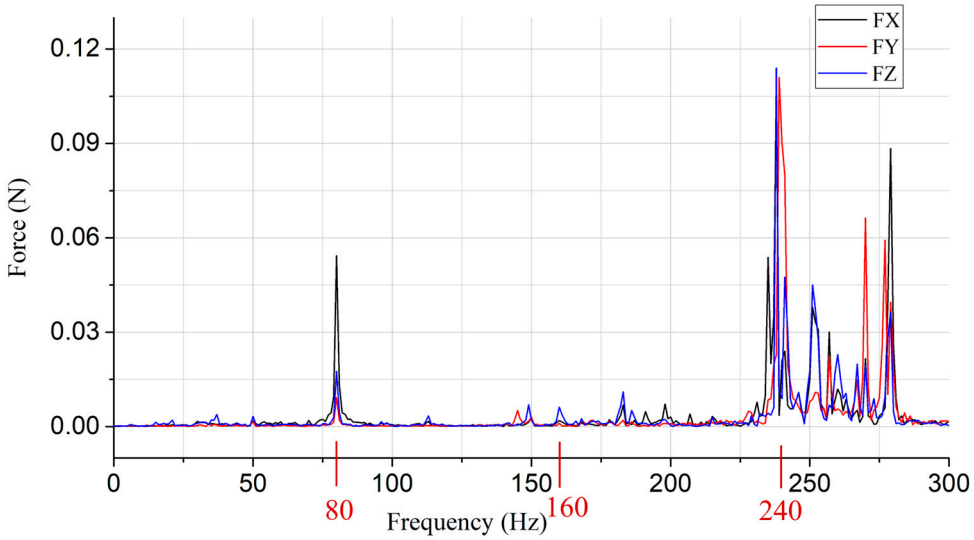


Figure 19. Measured frequency-domain response of the vibration force of the SC.

Moreover, the SC was delivered to CSST in December 2024. Subsequent integration and relevant optical imaging tests were completed, with the imaging quality meeting the specified requirements. This further validates the effectiveness of the microvibration suppression scheme.

5. Conclusions

The SC, a core instrument of the CSST, faces critical challenges from microvibrations generated by its internal shutter and the CCA, which degrade imaging resolution. This study presents a systematic microvibration suppression strategy integrating disturbance source control, payload isolation, and transfer path optimization to meet the strict requirements (vibration force $\leq$ 0.4 N, torque $\leq$ 0.1 N·m within 8–300 Hz).

The CCA adopts four PTCs, whose cold ends have no moving parts, resulting in lower vibration. The compressors utilize symmetric piston arrangements and real-time vibration cancellation algorithms, reducing the vibration of each compressor. Meanwhile, vibration isolators featuring a combined design of hydraulic damping and flexible structures are installed between the CCA and the SST. These isolators achieve over 95% vibration suppression efficiency, confining the post-isolation root-mean-square (RMS) force to 0.20 N. The shutter employs a dual-blade rotating structure, with shutters on both sides symmet-

rically arranged. Counterweights balance the moment of inertia of the blades on both sides to cancel out driving torque and in-plane vibration force. A sinusoidal drive control strategy ensures smooth operation during start-up and shutdown, and the residual low-frequency vibrations can be effectively compensated by the FSM, thus having no impact on camera imaging.

As the main vibration transmission path of the camera, the SST is integrally formed using M55J carbon fiber composite material. By optimizing the layout of reinforcing ribs and carbon fiber layup parameters, the structural dynamic characteristics are adjusted to reduce resonance peaks within the vibration frequency range of the CCA. Analysis after optimization shows that the root mean square (RMS) force and torque at the SC-CSST interface are 0.19 N and 0.06 N·m, respectively. This result validates that the optimized design of the SST's dynamic characteristics has effectively mitigated the risk of resonance amplification, ensuring the stability of vibration in the transmission path.

System-level tests on the integrated SC confirmed that the RMS vibration force and torque within 8–300 Hz are 0.25 N and 0.08 N·m, respectively, meeting design specifications. Further verification through optical imaging tests after integration with the CSST confirmed the effectiveness of the microvibration suppression scheme.

Author Contributions: Conceptualization, R.J., A.Z. and W.L.; methodology, R.J., T.J., C.L. and W.L.; software, H.S.; validation, R.J., Y.Z. (Yongchao Zhang), X.L., S.L., Z.L., H.W., S.G., L.W. and C.L.; formal analysis, R.J.; investigation, R.J. and T.J.; resources, E.L.; data curation, R.J. and C.L.; writing—original draft preparation, R.J.; writing—review and editing, A.Z. and W.L.; visualization, L.W.; supervision, A.Z. and J.D.; project administration, W.X. and Y.Z. (Yanqing Zhang); funding acquisition, A.Z. All authors have read and agreed to the published version of the manuscript.

Funding: This work was supported by the Manned Space Engineering Project of China.

Data Availability Statement: Data may be available from the corresponding author upon reasonable request and with appropriate approvals.

Acknowledgments: We would like to express our sincere gratitude for the support provided by all institutions and individuals who have contributed to the completion of this work. Special thanks are extended to the Shanghai Institute of Technical Physics Chinese Academy of Sciences (CAS), as they have offered valuable experimental resources and technical assistance for this research. We also wish to convey our special appreciation to the China Manned Space Agency (CMSA): its overall leadership and sustained support throughout the CSST mission have served as a fundamental guarantee for the development of the SC.

Conflicts of Interest: Author Hongyu Wang was employed by the companyChangchun Aerospace Composite Materials Co., Ltd. The remaining authors declare that the re-search was con-ducted in the absence of any commercial or financial relationships that could be construed as a potential conflict of interest.

References

1. De Bruijne, J.; Kohley, R.; Prusti, T. Gaia: 1000 Million Stars with 100 CCD Detectors. In Proceedings of the Space Telescopes and Instrumentation 2010: Optical, Infrared, and Millimeter Wave, San Diego, CA, USA, 27 June–2 July 2010; SPIE: Bellingham, WA, USA, 2010; Volume 7731, pp. 395–409.
2. Zhan, H. The Wide-Field Multiband Imaging and Slitless Spectroscopy Survey to Be Carried out by the Survey Space Telescope of China Manned Space Program. *Chin. Sci. Bull. (Chin. Version)* **2021**, *66*, 1290–1298. [CrossRef]
3. Greene, T.; Beichman, C.; Gully-Santiago, M.; Jaffe, D.; Kelly, D.; Krist, J.; Rieke, M.; Smith, E.H. NIRCam: Development and Testing of the JWST near-Infrared Camera. In Proceedings of the Space Telescopes and Instrumentation 2010: Optical, Infrared, and Millimeter Wave, San Diego, CA, USA, 27 June–2 July 2010; SPIE: Bellingham, WA, USA, 2010; Volume 7731, pp. 113–121.
4. Laborie, A.; Davancens, R.; Pouny, P.; Vétel, C.; Chassat, F.; Charvet, P.; Garé, P.; Sarri, G. The Gaia Focal Plane. In Proceedings of the Focal Plane Arrays for Space Telescopes III, San Diego, CA, USA, 28 August 2007; SPIE: Bellingham, WA, USA, 2007; Volume 6690, pp. 90–101.

5. Argabright, V.S.; VanCleve, J.E.; Bachtell, E.E.; Hegge, M.J.; McArthur, S.P.; Dumont, F.C.; Rudeen, A.C.; Pullen, J.L.; Teusch, D.A.; Tennant, D.S.; et al. *The Kepler Photometer Focal Plane Array*; Oschmann, J.M., Jr., de Graauw, M.W.M., MacEwen, H.A., Eds.; SPIE: Bellingham, WA, USA, 2008; p. 70102L.
6. Holz, J.M.; Kunt, C.; Lashley, C.; McGuffey, D.B. Development of a Lightweight Near-Zero CTE Optical Bench for the Wide-Field Camera 3 Instrument. In Proceedings of the Future EUV/UV and Visible Space Astrophysics Missions and Instrumentation, Waikoloa, HI, USA, 22–23 August 2002; SPIE: Bellingham, WA, USA, 2003; Volume 4854, pp. 435–446.
7. Li, L.; Wang, L.; Yuan, L.; Zheng, R.; Wu, Y.; Sui, J.; Zhong, J. Micro-Vibration Suppression Methods and Key Technologies for High-Precision Space Optical Instruments. *Acta Astronaut.* **2021**, *180*, 417–428. [CrossRef]
8. Yang, Z.; Yang, N.; Yu, Y. Earth-Observation Satellite Attitude Control Using Passive and Active Hybrid Magnetically Suspended Flywheels. *J. Beijing Inst. Technol.* **2014**, *23*, 226–234.
9. Li, L.; Tan, L.; Kong, L.; Yang, H.; Wang, D. Flywheel Micro-Vibration Characters of a High Resolution Optical Satellite. *J. Vibroengineering* **2017**, *19*, 3981–3993. [CrossRef]
10. Genolet, L.; Bozzo, E.; Paltani, S.; Autissier, N.; Larcheveque, C.; Thomas, C. The Read-out Shutter Unit of the Euclid VIS Instrument. In Proceedings of the Space Telescopes and Instrumentation 2016: Optical, Infrared, and Millimeter Wave, Edinburgh, UK, 26 June–1 July 2016; SPIE: Bellingham, WA, USA, 2016; Volume 9904, pp. 316–324.
11. Larchevêque, C.; Genolet, L.; Bozzo, E.; Paltani, S.; Manzoni, D.; Castelli, M.; Heurteau, J.P.; Thomas, C.; Constant, J.; Michaud, R. The Euclid VIS Read-out Shutter Unit: A Low Disturbance Mechanism at Cryogenic Temperature. *arXiv* **2018**, arXiv:1801.07496. [CrossRef]
12. Wang, X.; Yue, X.; Dai, H.; Yuan, J. Vibration Suppression for Post-Capture Spacecraft via a Novel Bio-Inspired Stewart Isolation System. *Acta Astronaut.* **2020**, *168*, 1–22.
13. Yuan, Q.; Liu, Y.; Qi, N. Active Vibration Suppression for Maneuvering Spacecraft with High Flexible Appendages. *Acta Astronaut.* **2017**, *139*, 512–520. [CrossRef]
14. Park, Y.-H.; Jo, M.-S.; Kim, H.-Y.; Oh, H.-U. Characteristics of Force Transmissibility in PLOVIS-II Cooler Micro-Vibration Isolation System. *Aerospace* **2025**, *12*, 511. [CrossRef]
15. Yasuda, S.; Takei, Y.; Okamoto, A.; Yanagase, K.; Watanabe, K.; Yoshida, S. Vibration Isolation System for Cryocoolers on the XRISM. *J. Astron. Telesc. Instrum. Syst.* **2025**, *11*, 42004. [CrossRef]
16. Komatsu, K.; Uchida, H. Microvibration in Spacecraft. *Mech. Eng. Rev.* **2014**, *1*, SE0010. [CrossRef]
17. Wayer, J.K.; Castet, J.-F.; Saleh, J.H. Spacecraft Attitude Control Subsystem: Reliability, Multi-State Analyses, and Comparative Failure Behavior in LEO and GEO. *Acta Astronaut.* **2013**, *85*, 83–92. [CrossRef]
18. Jiang, R.; Zhang, A.; Li, Z.; Liu, E.; Wang, L.; Le, S.; Zhang, Y.; Zhang, H.; Wang, H.; Guan, S. Main Structure of the Survey Camera for CSST: A Paradigm for Structural Design of Large-Scale Complex Space Optical Instruments. *Aerospace* **2025**, *12*, 1036. [CrossRef]
19. Dang, H. Development of High Performance Moving-Coil Linear Compressors for Space Stirling-Type Pulse Tube Cryocoolers. *Cryogenics* **2015**, *68*, 1–18. [CrossRef]
20. Radebaugh, R. A Review of Pulse Tube Refrigeration. *Adv. Cryog. Eng. Part A B* **1990**, *35*, 1191–1205.
21. Ni, T.; Yang, B. Adaptive Active Vibration Control Method for Cryocooler Compressor in Space. *Chin. Space Sci. Technol.* **2017**, *37*, 63.
22. Liu, X.; Kong, X.; Shen, J.; Zhou, X. Vibration Isolator with Relaxation Type Damping for Micro-Vibration Isolation from Satellite Remote Sensors. *Opt. Precis. Eng.* **2017**, *25*, 2448–2453. [CrossRef]
23. Chen, P.C.; Bowers, C.W.; Content, D.A.; Marzouk, J.; Romeo, R.C. Advances in Very Lightweight Composite Mirror Technology. *Opt. Eng.* **2000**, *39*, 2320–2329. [CrossRef]
24. Jiang, R.; Liang, W.; Wang, L.; Su, H.; Zhang, Y.; Jiang, T.; Du, J.; Zhang, A. Microvibration Testing and Decoupling for Space Payloads with Large Inertia, High Stiffness, and Discrete Interfaces. *Sensors* **2025**, *25*, 7352. [CrossRef] [PubMed]

Disclaimer/Publisher's Note: The statements, opinions and data contained in all publications are solely those of the individual author(s) and contributor(s) and not of MDPI and/or the editor(s). MDPI and/or the editor(s) disclaim responsibility for any injury to people or property resulting from any ideas, methods, instructions or products referred to in the content.